Elastic Backbone Defines a New Transition in the Percolation Model

Cesar I. N. Sampaio Filho,[1,*] José S. Andrade, Jr.,[1,2] Hans J. Herrmann,[1,2] and André A. Moreira[1]
[1]*Departamento de Física, Universidade Federal do Ceará, 60451-970 Fortaleza, Ceará, Brazil*
[2]*Computational Physics for Engineering Materials, IfB, ETH Zurich, Schafmattstrasse 6, 8093 Zurich, Switzerland*

(Received 20 January 2018; published 24 April 2018)

The elastic backbone is the set of all shortest paths. We found a new phase transition at p_{eb} above the classical percolation threshold at which the elastic backbone becomes dense. At this transition in 2D, its fractal dimension is 1.750 ± 0.003, and one obtains a novel set of critical exponents $\beta_{eb} = 0.50 \pm 0.02$, $\gamma_{eb} = 1.97 \pm 0.05$, and $\nu_{eb} = 2.00 \pm 0.02$, fulfilling consistent critical scaling laws. Interestingly, however, the hyperscaling relation is violated. Using Binder's cumulant, we determine, with high precision, the critical probabilities p_{eb} for the triangular and tilted square lattice for site and bond percolation. This transition describes a sudden rigidification as a function of density when stretching a damaged tissue.

DOI: 10.1103/PhysRevLett.120.175701

Despite being one of the simplest and most studied models, classical percolation [1–4] still bears yet uncovered surprises. It is well known that at the percolation threshold p_c the shortest path between two opposite sides of the system is fractal, with a fractal dimension that is only known numerically to be $d_{sp} = 1.1307 \pm 0.0004$ [5–8] in two dimensions and increases with dimension, until becoming two at and above the critical dimension $d = 6$. In fact, the shortest path is not unique: several shortest paths can exist simultaneously and the set of all the shortest paths has been called the elastic backbone in the past [9] because it is the subset of the backbone that, when elongated, would give the first contribution to a restoring force. The elastic backbone indeed determines the first resistance that is felt, when stretching damaged [10–12] or biological tissues [13–18] and thus has experimental relevance. It has been numerically established that at the percolation threshold p_c its fractal dimension is indistinguishable from the one of the shortest path [9]. Here, we report on the discovery that, above the classical percolation threshold p_c, there exists another critical probability $p_{eb} > p_c$ at which the elastic backbone becomes dense. While its dimension is known to be d_{sp} at p_c, our results in two dimensions show that it becomes unity between p_c and p_{eb}, it is 1.750 ± 0.003 at p_{eb}, and is equal to 2 above. At p_{eb}, we reveal critical scaling laws and a set of exponents, however, violating hyperscaling.

We simulated two-dimensional percolation configurations at occupation probability p for systems of size $L \times L$ with periodic boundary conditions in the horizontal direction and open boundaries at the top and bottom. Using the burning algorithm, we identified for each configuration the elastic backbone, i.e., the set of all shortest paths [9]. We considered site and bond percolation on the triangular lattice and on two types of square lattices, namely, tilted and nontilted. In Fig. 1, we see the elastic backbones for

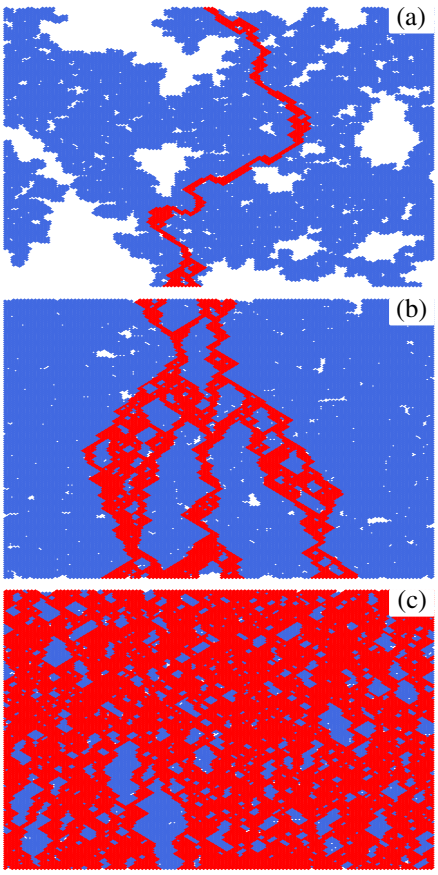

FIG. 1. Shown in red are typical elastic backbones obtained for site percolation on a tilted square lattice of linear size $L = 512$ and calculated with (a) $p = 0.6000$ ($p_c < p < p_{eb}$), (b) $p = 0.7055$ ($p = p_{eb}$), and (c) $p = 0.7500$ ($p > p_{eb}$). Occupied sites that are in the spanning cluster, but do not belong to the elastic backbone, are shown in blue. Other sites are represented in white.

 © 2018 American Physical Society

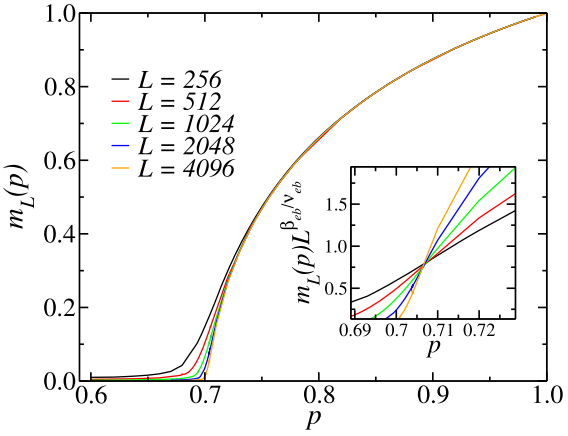

FIG. 2. Density $m_L(p)$ of the elastic backbone as a function of the occupation probability p for site percolation on the triangular lattice for different system sizes. (Inset) Determination of the threshold using finite-size scaling.

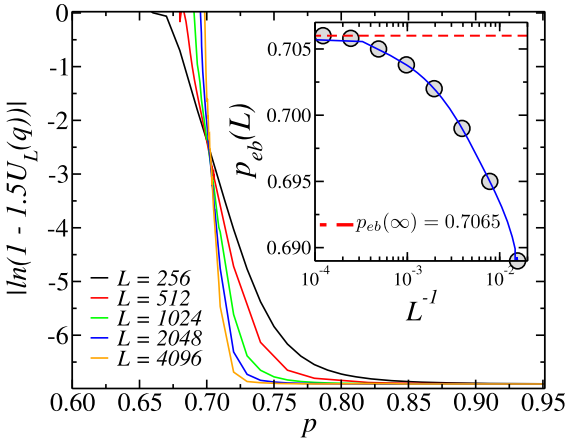

FIG. 3. Binder's cumulant $U_L(p)$ for different sizes L as a function of the occupation probability p for site percolation on the triangular lattice. (Inset) The dependence of $p_{\rm eb}(L)$ on L^{-1} for site percolation on the triangular lattice. $p_{\rm eb}(L)$ (circles) is obtained from the crossing point of U_L and U_{2L} for each pair of successive L values. Here, we consider $L = 64$, 128, 256, 512, 1024, 2048, 4096, and 8192. Extrapolating through the data points (blue line) to the thermodynamic limit, we obtain $p_{\rm eb}(\infty) = 0.7065 \pm 0.0004$ (red dashed line).

site percolation on a tilted square lattice for three different probabilities below, at, and above $p_{\rm eb}$.

We define the quantity $M_{\rm eb}$ as the mass of the elastic backbone, i.e., the number of sites that belong to the elastic backbone, and its density as $m_L(p) = \langle M_{\rm eb}\rangle/N$, where N is the total number of sites of the lattice. In Fig. 2, we plot $m_L(p)$ against $p > p_c$ for site percolation on the triangular lattice and find that there exists a clear phase transition at a value $p_{\rm eb} > p_c$ at which the elastic backbone becomes dense, with m acting as the order parameter of this transition. Using finite-size scaling, $p_{\rm eb}$ can be determined more precisely as shown in the inset, yielding also an estimate for the exponent $\beta_{\rm eb}/\nu_{\rm eb} = 0.25 \pm 0.02$. The threshold $p_{\rm eb}$ can be determined even more precisely using Binder's cumulant defined as

$$U_L(p) = 1 - \frac{\langle m_{\rm eb}^4\rangle}{3\langle m_{\rm eb}^2\rangle^2}. \tag{1}$$

In Fig. 3, we show the analysis of Binder's cumulant for site percolation on the triangular lattice, where we obtain $p_{\rm eb} = 0.7065 \pm 0.0004$. Moreover, by applying the same analysis, we find for site percolation $p_{\rm eb} = 1$ on the normal square lattice and $p_{\rm eb} = 0.7055 \pm 0.0005$ on the tilted square lattice. For bond percolation, we obtain $p_{\rm eb} = 0.6448 \pm 0.0005$ on the tilted square lattice and $p_{\rm eb} = 0.6450 \pm 0.0004$ on the triangular lattice. At $p = 1$, for the square lattice, starting from a given node in the border, there is just one shortest path of size L reaching the other side. In this way, the square lattice leaves the dense phase for any fraction of nodes removed. For the triangular and tilted lattices, on the other hand, there are 2^L different shortest paths (of size L) reaching the other side. This much larger number of shortest paths increases the mass of the elastic backbone, and therefore the triangular and tilted lattices remain dense, even after some sites have been removed. It should be noted that a similar dependence on the lattice is observed in other models. In the case of rigidity percolation [19–22], a transition on the triangular lattice is observed at finite p, while rigidity is only attained at $p = 1$ for the square lattice [23–25].

The fractal dimension d_f of the elastic backbone is obtained directly from the double-logarithmic plot of the mass of the elastic backbone $M_{\rm eb}$ against the linear size L of the considered lattice, at the threshold $p_{\rm eb}$. We find that the elastic backbone is fractal with a fractal dimension $d_f = 1.750 \pm 0.003$ for all studied models, while for $p_c < p < p_{\rm eb}$, it is one-dimensional, as shown in Fig. 4. In this case, although the spanning cluster is dense, the existence of various holes prevents the effective coalescence of the shortest paths present in the system, therefore leading to an elastic backbone, which is a fractal. At the threshold $p_{\rm eb}$, the exponent β/ν is then obtained from the relation $\beta/\nu = d - d_f$, resulting, for all studied models, in $\beta/\nu = 0.250 \pm 0.003$. Moreover, the response function of the order parameter, i.e., what would correspond in magnetic systems to the susceptibility, $\chi = N(\langle m_{\rm eb}^2\rangle - \langle m_{\rm eb}\rangle^2)$, diverges at the critical threshold $p_{\rm eb}$ with an exponent $\gamma_{\rm eb}/\nu_{\rm eb} = 1.00 \pm 0.02$ for all models considered, as shown in Fig. 5 for site percolation on the tilted square and triangular lattices. Finally, we also perform a full finite-size scaling analysis for $m_L(p)$ and for $\chi_L(p)$ of the form

$$m_L(p) = L^{-\beta_{\rm eb}/\nu_{\rm eb}}\tilde{m}(\varepsilon L^{1/\nu_{\rm eb}}), \tag{2}$$

$$\chi_L(p) = L^{\gamma_{\rm eb}/\nu_{\rm eb}}\tilde{\chi}(\varepsilon L^{1/\nu_{\rm eb}}), \tag{3}$$

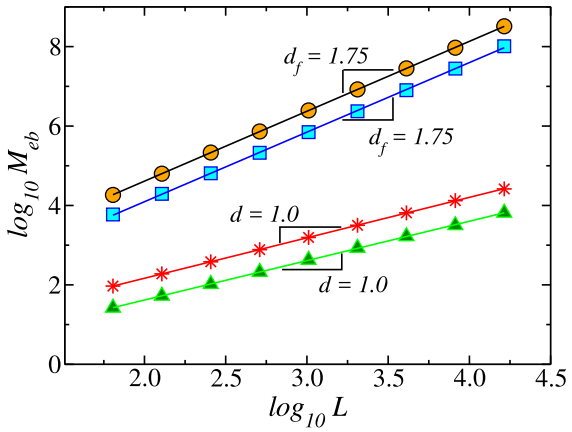

FIG. 4. Logarithmic plot of the mass $M_{\rm eb}$ of the elastic backbone as a function of the lattice size L for site percolation at $p_{\rm eb}$ on the tilted square lattice (orange circles) and on the triangular lattice (blue squares). The same is shown for the value of $p = 0.63$, between p_c and $p_{\rm eb}$, on the tilted square lattice for site percolation (red stars) and for bond percolation (green triangles), with L ranging from 64 to 16384 sites. At $p = p_{\rm eb}$, the least-squares fit to the data of a power law, $M_{\rm eb} \sim L^{d_f}$, gives the exponent $d_f = 1.7500 \pm 0.0003$ for the tilted square lattice (black line) and $d_f = 1.7500 \pm 0.0002$ for the triangular lattice (blue line). At $p = 0.63$ on the tilted square lattice, the least-squares fit to the data of a power law, $M_{\rm eb} \sim L^{d}$, gives the exponent $d = 1.0000 \pm 0.0002$ for site percolation (red line) and $d = 1.0000 \pm 0.0001$ for bond percolation (green line). In all cases, the errors are smaller than the symbols.

where $\varepsilon = (p - p_{\rm eb})$ is the distance from the critical threshold. The exponents $\beta_{\rm eb}/\nu_{\rm eb}$, $\gamma_{\rm eb}/\nu_{\rm eb}$, and $\nu_{\rm eb}$ are, respectively, associated with the decay of the order parameter, the divergence of the susceptibility, and the finite-size effects.

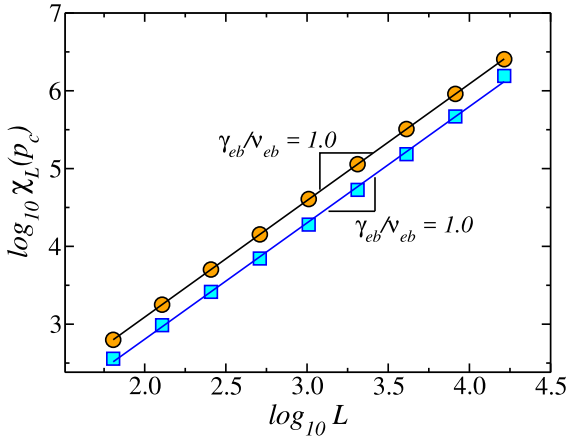

FIG. 5. Logarithmic plot of the susceptibility χ_L of the elastic backbone as a function of the lattice size L for site percolation at $p_{\rm eb}$, with L ranging from 64 to 16384 sites. The least-squares fit to the data of a power law, $\chi(p_{\rm eb}) \sim L^{\gamma/\nu}$, gives the exponent $\gamma/\nu = 1.00 \pm 0.01$ for the tilted square lattice (orange circles) and $\gamma/\nu = 1.00 \pm 0.02$ for the triangular lattice (blue squares).

As shown in Fig. 6, for the specific case of site percolation on the triangular lattice, we obtain excellent data collapse for values $\beta_{\rm eb} = 0.50 \pm 0.03$, $\gamma_{\rm eb} = 1.97 \pm 0.05$, and $\nu_{\rm eb} = 2.00 \pm 0.04$. We note that the hyperscaling relation $2\beta_{\rm eb} + \gamma_{\rm eb} = d\nu_{\rm eb}$ is violated [26,27]. Similar data collapse with the same exponents has been found for the other considered lattices.

We also studied the elastic backbone transitions on a lattice model that mixes the features of normal square and triangular lattices by adding to the normal square lattice with probability q some additional diagonals going from top left to bottom right. In this way, for $q = 0$, we obtain a normal square lattice and, for $q = 1$, a triangular lattice. For every value of $q > 0$, we found a value of $p_{\rm eb}(q) < 1$ at which the elastic backbone becomes dense. In Fig. 7(a) we show the finite-size scaling of the mass $M_{\rm eb}$ of the elastic backbone for site percolation at $p_{\rm eb}(q)$, for $q = 0.06$ and

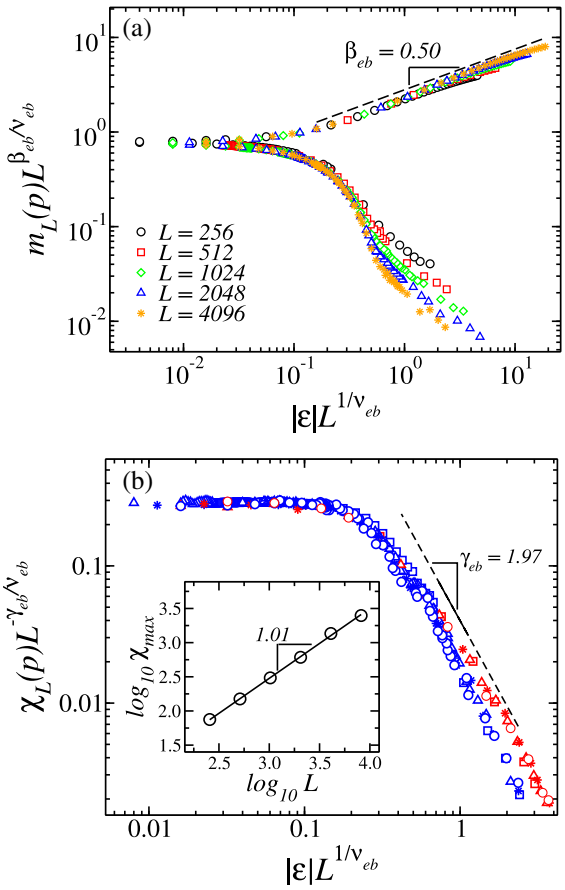

FIG. 6. (a) Results from the finite-size scaling analysis of the order parameter m_L obtained for site percolation on the triangular lattice. The growing and decaying curves correspond to values above and below $p_{\rm eb}$, respectively. The dashed line is the least-squares fit to data in the scaling region above $p_{\rm eb}$ for Eq. (2). (b) The same as in (a), but for the susceptibility χ_L. Blue symbols for $p < p_{\rm eb}$ and red symbols for $p > p_{\rm eb}$. Here, the dashed line has slope 1.97. (Inset) Log-log plot of the maximum of χ_L as a function of system size.

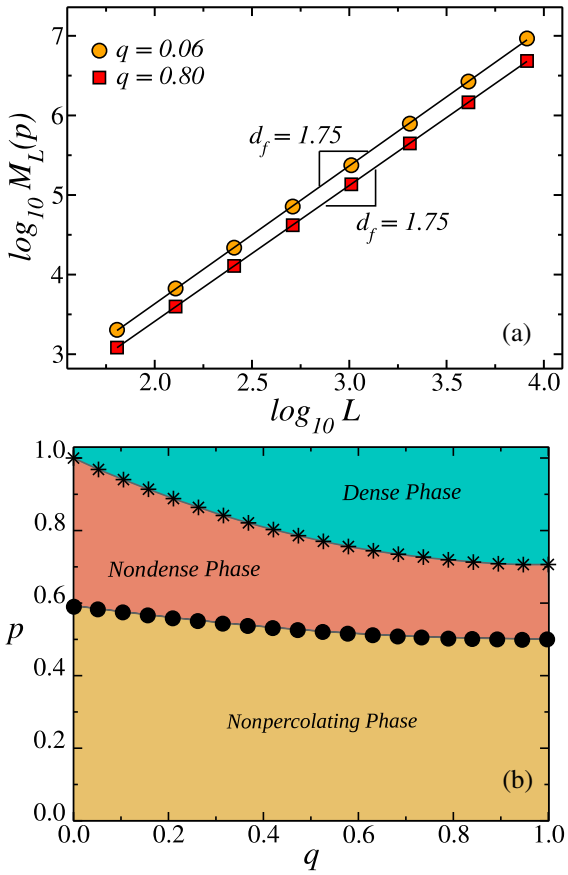

FIG. 7. (a) Logarithmic plot of the mass M_{eb} of the elastic backbone as a function of the lattice size L for site percolation at $p_{\mathrm{eb}}(q)$ for two different values of q. The least-squares fit to the data of a power law, $M_{\mathrm{eb}}[p_{\mathrm{eb}}(q)] \sim L^{d_f}$, gives the exponent $d_f = 1.750 \pm 0.005$ for $q = 0.06$ (orange circles) and $d_f = 1.750 \pm 0.003$ for $q = 0.80$ (red squares). The results show that the fractal dimension is within error bars the same for both cases. (b) Phase diagram between percolation probability p and the density of diagonals q. Three phases can be identified. The nonpercolating phase, where the spanning cluster is absent, bounded on top by the curve $p_c(q)$ (filled circles), which represents the classical percolation thresholds. The nondense phase is bounded by the curve $p_c(q)$ on the bottom and the curve $p_{\mathrm{eb}}(q)$ on the top (stars), which is the critical line along which the order parameter $m_L(p)$ vanishes and the elastic backbone is fractal. Finally, in the dense phase on the top, the elastic backbone becomes dense.

$q = 0.80$. The results show that the fractal dimension is, within error bars, the same for both cases. Moreover, we calculated these fractal dimensions at $p_{\mathrm{eb}}(q)$ for different values of $q > 0$ and found that they do not depend on q. This underlines, on one hand, the universality of d_{eb} and questions, on the other hand, any relation to rigidity percolation [19–22], which does exhibit a transition at an intermediate value of q. In Fig. 7(b), we show the phase diagram between percolation probability p and the density of diagonals q, where three phases are identified. In the nonpercolating phase, the spanning cluster is absent and, consequently, the elastic backbone does not percolate. The nonpercolating phase is bounded by the curve $p_c(q)$, which represents the classical percolation thresholds. The nondense phase is characterized by a linear scaling with L of the elastic backbone and it is bounded by the curves $p_c(q)$ on the bottom and $p_{\mathrm{eb}}(q)$ on the top, which defines the critical line along which the order parameter $m_L(p)$ vanishes and the elastic backbone is fractal. In the dense phase, the dimension of the elastic backbone is equal to the dimension of the lattice considered.

Concluding, we discovered that the mass of the elastic backbone serves as an order parameter for a new transition within the connected phase of classical percolation, exhibiting a new set of critical exponents $\beta_{\mathrm{eb}} \approx 1/2, \gamma_{\mathrm{eb}} \approx 2, \nu_{\mathrm{eb}} \approx 2$, and $d_f \approx 7/4$ in two dimensions. Interestingly, however, hyperscaling is violated, this being to our knowledge the first example for a violation of hyperscaling in a purely geometrical model. It would be also interesting to investigate higher dimensions and try to formulate a mean-field approximation. Similar transitions for elastic backbones could be expected in models with tunable disorders [28–36].

Our findings have direct consequences to the stretching of random fibrous materials like biological tissues: when the first restoring force is felt, the resistance will grow very gently with displacement below the threshold p_{eb}, while above p_{eb}, the system will then be instead very stiff. It is thus a transition between two very different stress-strain relations for a damaged tissue.

Furthermore, there exists an interesting similarity between the elastic backbone percolation, as introduced here, and the phase transition associated with rigidity percolation, since the stressed backbone [37–39] is a fractal whose dimension ($d_f = 1.78 \pm 0.02$) is very close to the fractal dimension of the elastic backbone at p_{eb}. For nontilted square lattices, in both cases, the transition is shifted to $p = 1$ [23–25]. Nevertheless, the two transitions describe different phenomena, since they are in general located at different threshold values and have a different set of critical exponents.

We thank the Brazilian agencies CNPq, CAPES, FUNCAP, the National Institute of Science and Technology for Complex Systems, and the European Research Council (ERC) Advanced Grant No. 319968 FlowCCS for financial support.

Note added.—P. Grassberger [40] and R. M. Ziff [41] pointed out to us that there seems to be a strong relation between our transition and the one of Directed Percolation.

*Corresponding author.
cesar@fisica.ufc.br

[1] S. R. Broadbent and J. M. Hammersley, Math. Proc. Cambridge Philos. Soc. **53**, 629 (1957).
[2] S. Kirkpatrick, Rev. Mod. Phys. **45**, 574 (1973).

[3] D. Stauffer and A. Aharony, *Introduction to Percolation Theory* (Tailor & Francis, London, 1985).
[4] M. Sahimi, *Applications of Percolation Theory* (Taylor & Francis Group, London, 1994).
[5] H. J. Herrmann and H. E. Stanley, J. Phys. A **21**, L829 (1988).
[6] P. Grassberger, J. Phys. A **25**, 5475 (1992).
[7] N. V. Dokholyan, Y. Lee, S. V. Buldyrev, S. Havlin, P. R. King, and H. E. Stanley, J. Stat. Phys. **93**, 603 (1998).
[8] M. E. J. Newman and R. M. Ziff, Phys. Rev. Lett. **85**, 4104 (2000).
[9] H. J. Herrmann, D. C. Hong, and H. E. Stanley, J. Phys. A **17**, L261 (1984).
[10] D. J. Jacobs and M. F. Thorpe, Phys. Rev. Lett. **75**, 4051 (1995).
[11] V. K. de Souza and P. Harrowell, Proc. Natl. Acad. Sci. U.S.A. **106**, 15136 (2009).
[12] L. Zhang, D. Z. Rocklin, L. M. Sander, and X. Mao, Phys. Rev. Mater. **1**, 052602 (2017).
[13] J. Bates, G. Maksym, D. Navajas, and B. Suki, Ann. Biomed. Eng. **22**, 674 (1994).
[14] H. Yuan, E. P. Ingenito, and B. Suki, J. Appl. Physiol. **83**, 1420 (1997).
[15] J. W. Baish and R. K. Jain, Cancer Res. **60**, 3683 (2000).
[16] B. Suki, Am. J. Respir. Crit. Care Med. **166**, 133 (2002).
[17] M. C. Ritter, R. Jesudason, A. Majumdar, D. Stamenović, J. A. Buczek-Thomas, P. J. Stone, M. A. Nugent, and B. Suki, Proc. Natl. Acad. Sci. U.S.A. **106**, 1081 (2009).
[18] F. E. Lennon, G. C. Cianci, N. A. Cipriani, T. A. Hensing, H. J. Zhang, C.-T. Chen, S. D. Murgu, E. E. Vokes, M. W. Vannier, and R. Salgia, Nat. Rev. Clin. Oncol. **12**, 664 (2015).
[19] Y. Kantor and I. Webman, Phys. Rev. Lett. **52**, 1891 (1984).
[20] W. Bresser, P. Boolchand, and P. Suranyi, Phys. Rev. Lett. **56**, 2493 (1986).
[21] C. Moukarzel, P. M. Duxbury, and P. L. Leath, Phys. Rev. Lett. **78**, 1480 (1997).
[22] W. G. Ellenbroek, V. F. Hagh, A. Kumar, M. F. Thorpe, and M. van Hecke, Phys. Rev. Lett. **114**, 135501 (2015).
[23] C. F. Moukarzel, Phys. Rev. Lett. **81**, 1634 (1998).
[24] A. Souslov, A. J. Liu, and T. C. Lubensky, Phys. Rev. Lett. **103**, 205503 (2009).
[25] X. Mao, N. Xu, and T. C. Lubensky, Phys. Rev. Lett. **104**, 085504 (2010).
[26] K. Binder and J.-S. Wang, J. Stat. Phys. **55**, 87 (1989).
[27] R. L. C. Vink, T. Fischer, and K. Binder, Phys. Rev. E **82**, 051134 (2010).
[28] M. Porto, S. Havlin, S. Schwarzer, and A. Bunde, Phys. Rev. Lett. **79**, 4060 (1997).
[29] L. A. Braunstein, S. V. Buldyrev, R. Cohen, S. Havlin, and H. E. Stanley, Phys. Rev. Lett. **91**, 168701 (2003).
[30] J. S. Andrade, E. A. Oliveira, A. A. Moreira, and H. J. Herrmann, Phys. Rev. Lett. **103**, 225503 (2009).
[31] S. Pradhan, A. Hansen, and B. K. Chakrabarti, Rev. Mod. Phys. **82**, 499 (2010).
[32] E. Fehr, D. Kadau, J. S. Andrade, and H. J. Herrmann, Phys. Rev. Lett. **106**, 048501 (2011).
[33] A. A. Moreira, C. L. N. Oliveira, A. Hansen, N. A. M. Araújo, H. J. Herrmann, and J. S. Andrade, Jr, Phys. Rev. Lett. **109**, 255701 (2012).
[34] A. Shekhawat, S. Zapperi, and J. P. Sethna, Phys. Rev. Lett. **110**, 185505 (2013).
[35] C. L. N. Oliveira, P. A. Morais, A. A. Moreira, and J. S. Andrade, Phys. Rev. Lett. **112**, 148701 (2014).
[36] C. I. N. Sampaio Filho, A. A. Moreira, N. A. M. Araújo, J. S. Andrade, Jr., and H. J. Herrmann, Phys. Rev. Lett. **117**, 275702 (2016).
[37] C. Moukarzel and P. M. Duxbury, Phys. Rev. Lett. **75**, 4055 (1995).
[38] D. J. Jacobs and M. F. Thorpe, Phys. Rev. Lett. **80**, 5451 (1998).
[39] C. Moukarzel and P. M. Duxbury, Phys. Rev. E **59**, 2614 (1999).
[40] P. Grassberger, J. Phys. A **22**, 3673 (1989).
[41] C. A. Voigt and R. M. Ziff, Phys. Rev. E **56**, R6241 (1997).